Available online at www.sciencedirect.com
SCIENCE DIRECT®

Journal of the European Ceramic Society 24 (2004) 2527–2535

www.elsevier.com/locate/jeurceramsoc

Flame assisted vapour deposition of cathode for solid oxide fuel cells. 2. Modelling of processing parameters

S. Charojrochkul*, R.M. Lothian[1], K.L. Choy[2], B.C.H. Steele

Department of Materials, Imperial College of Science, Technology and Medicine, London SW7, UK

Abstract

Flame assisted vapour deposition (FAVD) has been used to deposit porous lanthanum strontium manganese oxide (LSM) films for solid oxide fuel cell (SOFC) cathodes. The variation of microstructure of the deposited films with the processing parameters has been described in Part 1 of this paper. In parallel with the experiments, complementary modelling work of the turbulent flame was carried out using the finite volume CFD package FLUENT*. This was the first attempt in FAVD process modelling. The effects of varying experimental parameters such as the ratio of alcohol to water and the concentration of the precursor solution, have been investigated. The temperature distributions obtained from the modelling are consistent with the experimental results. The highest combustion temperature predicted from the model indicates the complete combustion process which yields powdery film in Part 1. Hence, the results in this paper confirm the trends for the experimental work.

Keywords: Cathodes; Flame assisted vapour deposition; Fuel cells; Modelling; SOFC

1. Introduction

Flame assisted vapour deposition (FAVD) has been exploited as a novel oxide ceramic film fabrication technique. Films fabricated via this technique include yttria stabilised zirconia (8 mol% Y_2O_3 in ZrO_2, YSZ),[1] barium titanate ($BaTiO_3$),[2] and lanthanum strontium manganese oxide ($La^x_1\_Sr^xMnO_3$, LSM).[3,4] Part 1 of this paper[5] reported the experimental results for the deposition of LSM films, and showed the effects of the following processing parameters: amount of fuel in the precursor solution, the concentration of the precursor, the flow rate of the precursor, the pressure of the compressed air used in atomising the precursor solution, and the distance between the spray nozzle and the substrate.

Mathematical modelling is a cost-effective way to supplement experimental work or assist in process design. Modelling of the deposition process has been applied to the chemical vapour deposition (CVD) technique.[6–8] However, these models were not applicable to other types of processing technique. There were also some commercially available models for CVD[9] and thermal spray techniques. There was only one paper on the chemistry model in combustion CVD in which the focus was not on the processing parameters.[10] Nevertheless, no relevant modelling work on the process parameters of FAVD has been reported in the literature.

This is the first attempt to model FAVD. The combustion process was modelled using FLUENT, which has the facility to deal with the processes governing chemical reactions in a turbulent flame. The simulation produced a 2D contour map of the relevant physical and chemical quantities, in which the temperature was signified as the most critical parameter. The effect of changing a number of processing parameters was simulated. It was then possible to predict the effect of such changes on the deposition process, which was governed by the conditions prevailing in the flame.

In order to streamline the modelling process, some approximations and simplifications of the actual experiment were introduced. Hence, detailed quantitative agreement with experiment was not expected. Instead, the model had the following goals. Firstly, to obtain qualitative agreement with experiment in terms of the response to variation of key processing parameters. Secondly, to

* Corresponding author at present address: National Metal and Materials Technology Center, Bangkok, Thailand. Tel.: +66-2-564-6500; fax: +66-2-564-6447.
E-mail address: sumittrc@mtec.or.th (S. Charojrochkul).
[1] Present address: Department of Computer and Mathematical Sciences, The Robert Gordon's University, Aberdeen, UK.
[2] Present address: School of Mechanical, Materials, Manufacturing Engineering and Management, Faculty of Engineering, University of Nottingham, UK.

0955-2219/$ - see front matter © 2003 Elsevier Ltd. All rights reserved.
doi:10.1016/j.jeurceramsoc.2003.08.008

gain a better understanding of the experimental results. Finally, to test the feasibility of modelling FAVD, before sinking substantial resources into an attempt to obtain close quantitative agreement with experiment.

2. Experimental setup

FAVD involves many chemical processes and the apparatus consisted of many components i.e. a flame source, spray nozzle, precursor flow control, air compressor, air flow control, hot plate, and temperature measurement unit. A liquid precursor, mainly ethanol and water mixed with soluble metal salts of required cations, was atomised through the spray nozzle by means of compressed air. The atomised precursor was in the form of fine droplets, which are assumed to be in the form of an aerosol. These droplets then combusted when ignited by a flame source. The heat of combustion provided thermal energy during the decomposition and vapourisation of these droplets, which underwent vapour phase reactions, resulting in an oxide film being deposited on a substrate surface underneath the spray nozzle. The substrate was placed on a hot plate, which provided thermal environment in addition to the flame source.

All of these experiments were carried out in an open atmosphere with no physical barriers apart from the substrate located on a hot plate underneath the spray nozzle. The flow rates of the compressed air and the liquid precursor were measured. The temperature at the substrate surface was monitored throughout the deposition. The ratio of ethanol to water in the liquid precursor was varied together with the pressure of the compressed air. This experimental part was carried out as described in part 1 of this paper.

3. Model geometry

It was found convenient to model the experiment as an axisymmetric cylinder, 25 cm high and 15 cm in radius. The model was a horizontal cylinder with an inlet at the bottom left corner which represented the air nozzle at the top in real experiments. This was slightly larger than the real experimental setup, to prevent flow deflected by the hot plate from disrupting the flame. Fuel and air were injected along the axis of symmetry from an inlet on the top face of the cylinder which was shown as the left corner in the model. This inlet represented separate fuel and air nozzles. At the opposite side to the inlet was the hot plate, which was set to a temperature of 227 °C at its centre. The deposition occurred on the substrate at the surface of this hotplate. All other boundaries were treated as outlets at atmospheric pressure because our experiment was carried out in an open atmosphere. Fig. 1 shows a typical computational grid (25 × 20 cells) used for this setup comparing with the real experimental setup. The geometry used in this model was similar to the real experimental setup with only assumption on the droplet size (one of the modelled parameter).

4. Physical processes and theory

FLUENT uses a finite volume approach to solve the Navier-Stokes equations for viscous fluid flow in addition to the basic conservation equations, in this case the fluid is considered incompressible. Since the precursor was atomised in the real system on exit from the spray nozzle, the fuel spray coming out of the inlet was treated as a dispersed secondary phase of liquid droplets. The droplets then evaporated into the primary gas phase and underwent combustion when ignited by the flame source. During vapourisation, the rate of vapourisation is governed by gradient diffusion, with the flux droplet vapour into the gas phase related to the gradient of the vapour concentration between the droplet surface and the bulk gas. The heat change in the droplet during vapourisation includes the convective and latent heat transfer between the droplet and the gas.

The k–ε model was used to deal with the turbulent nature of the flame including shear flows and wall-bounded flows. Since turbulence strongly affects transport processes, including diffusion, it must be taken into account when considering chemical reactions. This model is an eddy–viscosity model in which the Reynolds stresses are assumed to be proportional to the mean velocity gradients, with the constant of proportionality being the turbulent viscosity, μ_t. This assumption is known as the Boussinesq hypothesis with the following expression for the Reynolds stresses:[11]

$$\rho\overline{u_i' u_j'} = \rho\frac{2}{3}k\delta_{ij} - \mu_t\left(\frac{\partial u_i}{\partial x_j} + \frac{\partial u_j}{\partial x_i}\right) + \frac{2}{3}\mu_t\frac{\partial u_l}{\partial x_l}\delta_{ij} \quad (1)$$

where k is the turbulent kinetic energy:

$$k = \frac{1}{2}\sum_i \overline{u_i'^2} \quad (2)$$

The turbulent viscosity, μ_t, plays the same role as the molecular viscosity. However, μ is replaced by an effective viscosity, μ_{eff}:

$$\mu_{eff} = \mu + \mu_t \quad (3)$$

The turbulent viscosity is assumed to be proportional to the product of a turbulent velocity scale and length scale. These velocity and length scales are obtained from two parameters: k, the turbulent kinetic energy and ε, the dissipation rate of k. The velocity scale is $\sqrt{k}$ and the length scale is $\frac{\sqrt{k^3}}{\varepsilon}$. μ_t then becomes:

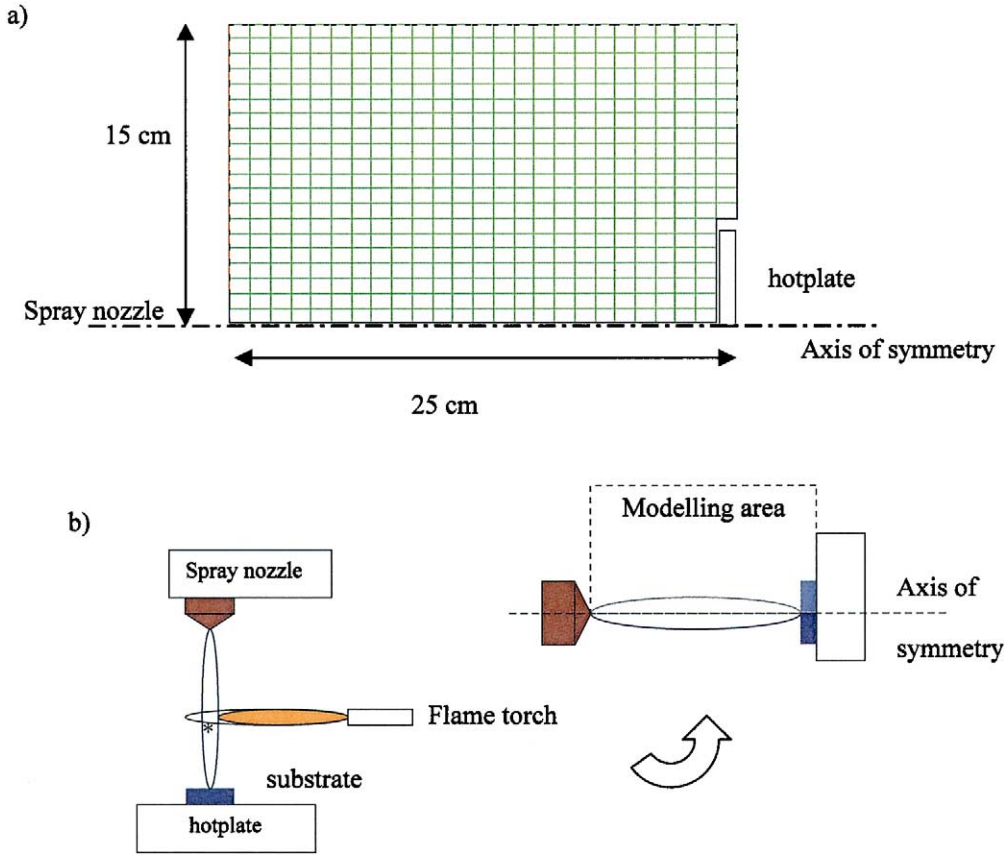

Fig. 1. (a) A computational grid of the model setup and (b) A real experimental setup.

$$\mu_t = \rho C_\mu \frac{k^2}{\varepsilon} \quad (4)$$

where C_μ is an empirically derived constant of proportionality.

FLUENT uses a mixture fraction model of the combustion process, combined with a probability density function approach to simulate the effect of turbulent fluctuations.[12]

$$f = \frac{m_F}{m_F + m_O} \quad (5)$$

where f is a mixture fraction, subscripts F and O denote the mass of the fuel and the oxidant inlets.

Individual species transport equations are not solved. Instead, a single conserved scalar, the mixture fraction, is calculated and individual component concentrations are derived from the predicted mixture fraction distribution. This model has been specifically developed for the simulation of turbulent diffusion flows, for which it offers many benefits. The turbulence effects in the conserved scalar approach are accounted for with the help of a probability density function or PDF. The reacting system is treated via chemical equilibrium calculations. Physical properties of chemical species and equilibrium data are obtained from a chemical database. The mixture fraction method allows intermediate species formation, dissociation effects, and the coupling between turbulence and chemistry to be accounted for in a rigorous way. It allows quite accurate estimation of the flow field mean density.

This approach requires the calculation of probability density functions, which is carried out by the preprocessor PrePDF*. PrePDF accesses a database of thermodynamic properties, which does not currently include data for ethanol. For this reason, a methanol/water mixture was substituted for the actual ethanol/water mixture as fuel. The deviation influenced by this approximation on the results was likely to have been less than that caused by other approximations i.e. simplified geometry and uncertainty regarding the exact spectrum of droplet sizes. Qualitative trends should be the same for the two alcohols from their thermodynamic properties.

5. Boundary conditions

FLUENT applies boundary conditions by using artificial boundary cells of various types.[13] The types used here were 'wall', 'inlet', 'outlet', and 'symmetry' boundaries, as shown in Fig. 2.

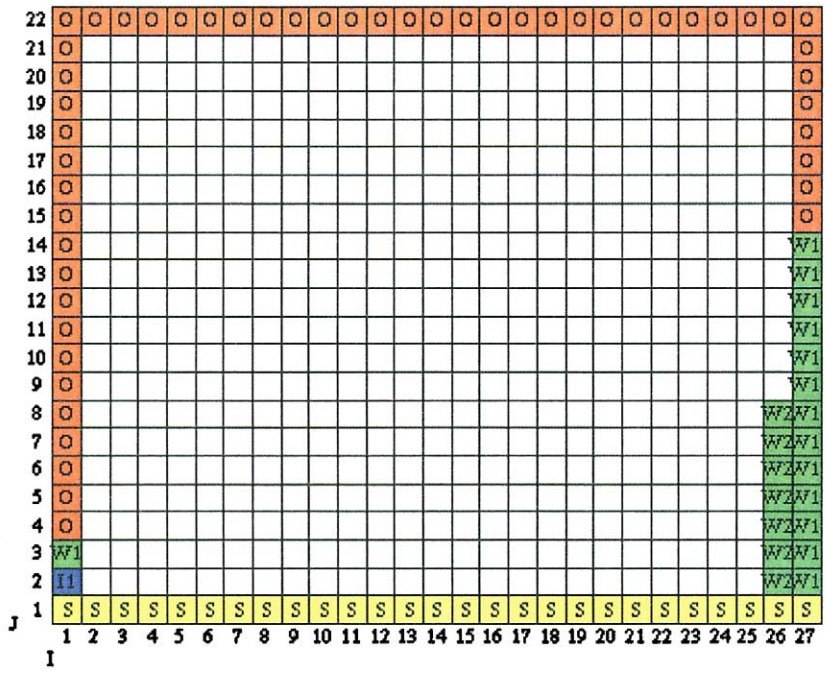

Fig. 2. Boundary conditions of the model used in this paper.

The surface of the hot plate (substrate position) is a wall boundary, where the normal velocity component is constrained to zero. For a turbulent flow, it is a standard practice to use empirical 'wall functions' at the near wall grid point to estimate the effect of the wall on the turbulent flow. This eliminates the need to fully resolve all regions of a turbulent boundary layer and allows the near wall grid point to be placed relatively far from the wall. This approach helps saving the computational resources in turbulent flow simulations for the standard high-Reynolds-number.

Appropriately, the axis of symmetry, inlet and outlet are boundaries of symmetry, inlet and outlet types respectively. At the axis of symmetry, the radial flow velocity is zero and the radial derivatives of all other variables vanish. These conditions are necessary to avoid unphysical singularities at the axis. At the inlet, the velocity, temperature and composition of the primary phase flow were specified. The k–ε model also required an estimate of the intensity and characteristic length of the turbulence in the incoming flow. The dispersed secondary phase was also introduced at the inlet with a given composition, range of velocities, and spectrum of droplet size. The droplet size spectrum turned out to be a crucial process parameter. At the outlet, combusted vapours were exhausted at atmospheric pressure. Values for all variables at the outlet boundary were extrapolated from the interior cells adjacent to the outlet. More details of the model may be found in the author's thesis.[14]

6. Modelling approaches

In Part 1 of this paper, five processing parameters which affect the microstructure and properties of the deposited films are the ratio of ethanol to water, the flow rate of the precursor, the air atomiser pressure, distance from the spray nozzle to the substrate, and the concentration of the precursor. During each deposition, the particular shape of the combustion flame roughly indicated the types of microstructure to be expected as explained in Part 1. Using preliminary modelling results and physical arguments, three key process parameters were identified for modelling.

6.1. Effect of mixture fraction

Apparently, the amount of fuel in the fuel/air mixture had a strong effect on the reaction. In the experiment this was adjusted by altering *the mass flow rate* through the fuel nozzle and *the air atomiser pressure*. In the model, this 'mixture fraction' was set at the inlet.

6.2. Effect of amount of alcohol

The *ratio of alcohol to water* in the liquid precursor (the fuel in the model) also affected the mixture of reactants available for combustion. The amount of alcohol was included in the mixture fraction in the model.

6.3. Effect of droplet size

Finally, the size of liquid droplets determined their rate of evaporation, which influenced the speed at which gaseous fuel was supplied to the combustion process. The droplet size is varied by adjusting *the flow rate* of precursor and *the air atomiser pressure* in the experimental part.

Eventually, the mixture fraction at the inlet, the proportion of alcohol in the fuel and the droplet size spectrum closest to real experiments were chosen as the parameters of this study. Since the set geometry of the reaction is larger than the real experimental setup, the distance between the spray nozzle to the substrate can be shown from the temperature contours.

7. Results and discussion

The maximum flame temperature was selected as the principal output parameter of the study. The flame shape and size were indicated by temperature contour maps. Some observations were made regarding to the chemical composition of the gaseous phase.

7.1. Effect of mixture fraction

The temperature contours at different mixture fractions (m.f.) from 0.05 to 0.5 for a 70% alcohol solution are shown in Fig. 3. The temperature range in each figure is defined in a control legend beside each contour. The maximum temperature is indicated in red while the minimum temperature is indicated in blue. The maximum temperatures for each mixture fraction are plotted in Fig. 4.

The length of red, hot flame area represents the region of intense combustion. If the red area is elongated, this means that intense combustion occurs over a longer distance and hence, over a greater length of time. The area beyond the red area is where the combustion completed. At this point, all species in the vapour phase have undergone a gas phase homogeneous reaction, by which oxide powders are obtained experimentally.[1]

In Fig. 3(a) and (b), the maximum temperature occured at 14–16 cm from the nozzle, thus combustion completed well before reaching the hot plate (and the substrate). From the results of Part 1, it can be deduced that only a powdery film would be deposited. Conversely, in Fig. 3(c)–(f), the combustion of the fuel still continued at the substrate. Therefore, some non-combusted vapour must reach the substrate. This led to a heterogeneous reaction, which resulted in either a dense oxide film or a porous film by the interaction between species in the vapour phase and solid phase nucleation.

A high maximum temperature was desirable as it signified complete combustion. From Fig. 4, the highest temperature occurred at a mixture fraction of 0.1 and that the temperature fell off sharply above 0.3, presumably due to a shortage of oxygen (as oxidant).

The above results suggested optimum processing conditions occur when the mixture fraction was 0.1 and the substrate was placed at 15 cm underneath the spray nozzle while the distance between the spray nozzle and the substrate was set at 12 cm in real experiments. Since complete combustion took place at a distance around 14–16 cm, the substrate placing at shorter distance would allow heterogeneous reaction to occur resulting in dense or porous films. The effect of mixture fraction also indicated the same trend of results as observed by Hunt[15] for the effect of oxygen content. The maximum flame temperature increased with the increase of oxygen content in the atomising gas. The shape of flame described also matched the temperature contours in this paper.

The maximum temperature from modelling work was around 1600 °C in Fig. 3(b). However, the maximum flame temperature from experiments never exceeded 1300 °C, possibly due to the thermodynamic properties difference of the alcohol used (ethanol in experimental work) and the addition of metal salts. Other approximations and uncertainties involved in the modelling process might be responsible.

7.2. Effect of amount of alcohol

The comparison of maximum temperatures among selected mixture fractions, using 50%, 70%, and 80% alcohol solutions was plotted in Fig. 5. The combustion length and temperature were low for the low fuel and much greater for the high fuel fractions. From all the observations, the shapes of the temperature contours at various mixture fractions did not differ much in the low fuel models but showed significant changes in the high fuel models. Only at the mixture fraction of 0.3 of 80% alcohol solution was the maximum combustion temperature at the substrate, while in other conditions the combustion was completed prior to reaching the substrate. These observations could be explained in the same way as for the effect of mixture fractions. Note that 70% alcohol led to the greatest maximum temperatures in which this parameter was much more sensitive to changes in alcohol content than to changes in mass fraction. Hence, it was important to control the alcohol content closely. Fortunately, it was easier to do this than to control the mass fraction, which could only be indirectly controlled.

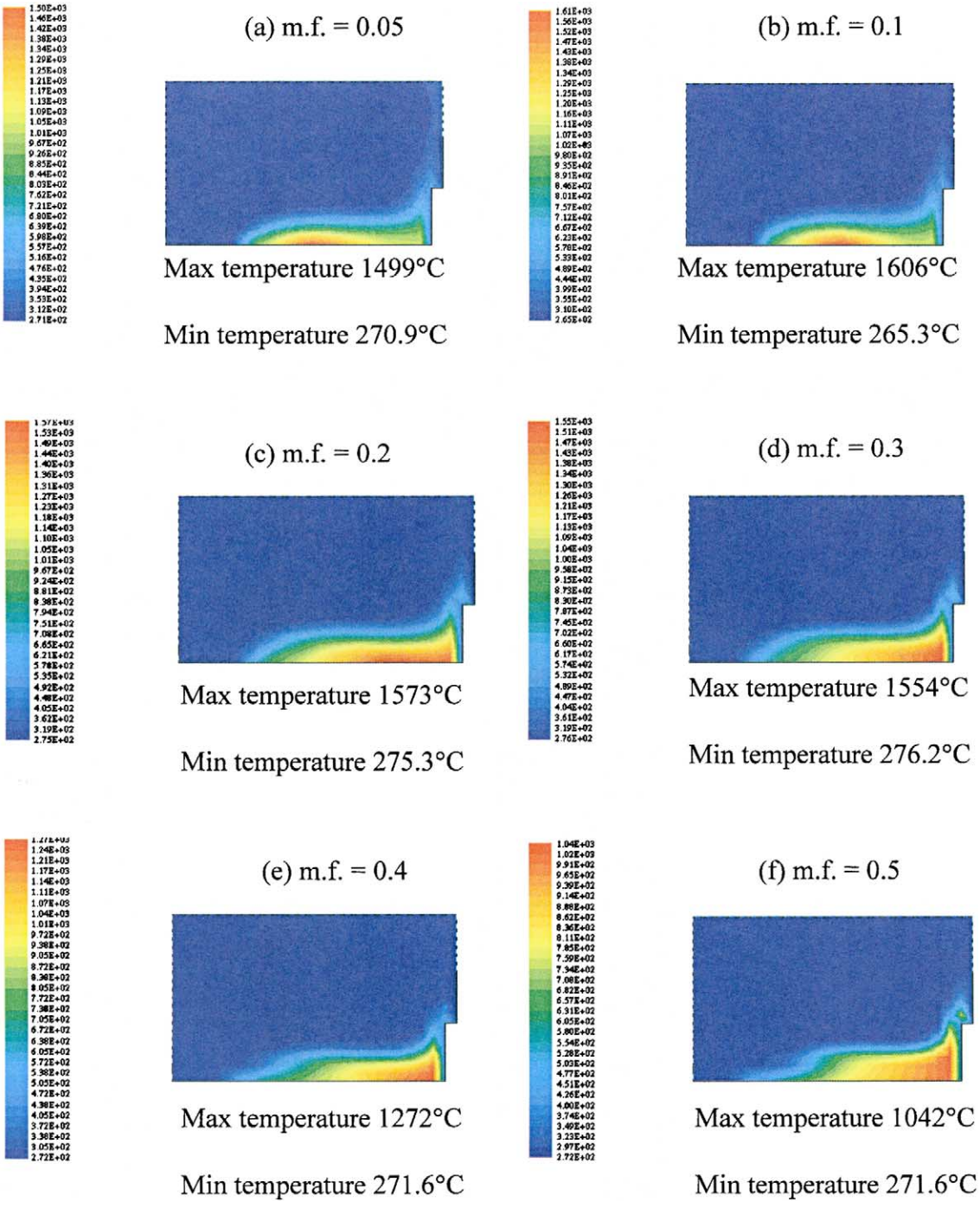

Fig. 3. Temperature distribution contours at different mixture fractions for 70% alcohol solution.

Additional insight may be gained by considering the chemical species involved in the reaction. The amounts of chemical species from the combustion process were compared for 50, 70 and 80% ethanol in the precursor while the mixture fraction was fixed at 0.2. The chemical species detected were oxygen gas, water, carbon monoxide and carbon dioxide. The maximum and minimum mass fractions of each gas were summarised in Fig. 6.

The reaction below describes the complete combustion reaction taking place between the spray nozzle and the substrate as in this model.

$$CH_3OH + \tfrac{3}{2}O_2 \rightarrow 2H_2O + CO_2 \quad (A)$$

At the same time, CO and CO_2 coexist at equilibrium, as in reaction B.

$$2CO + O_2 \leftrightarrow 2CO_2 \quad (B)$$

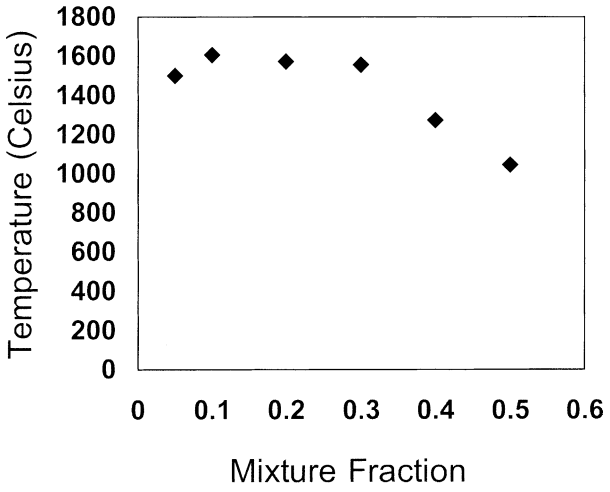

Fig. 4. Maximum temperature versus mixture fraction for the 70% alcohol.

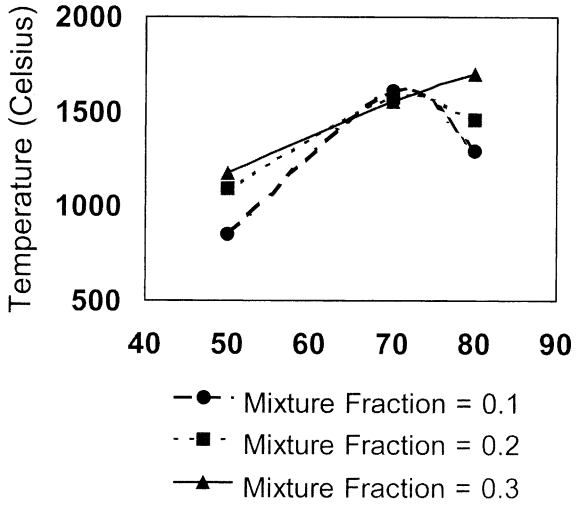

Fig. 5. The maximum temperature for various percentages of alcohol and mixture fractions.

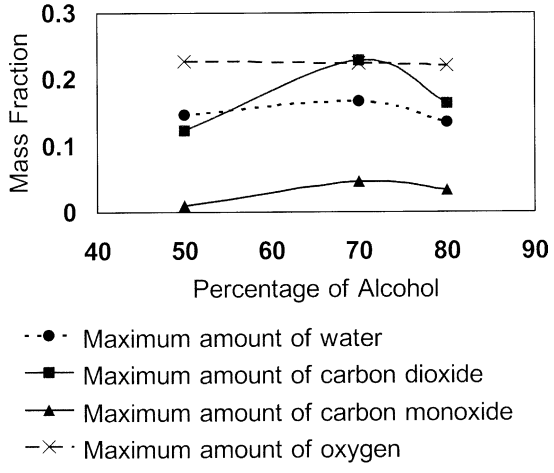

Fig. 6. Mass fraction of chemical species present for 50, 70, and 80% alcohol mixtures.

From these two reactions, water and carbon dioxide are the products of the complete combustion process. The combustion process is turbulent, and the reactions involved are not at equilibrium. The amounts of all species involved in the reactions are compared in Fig. 6. From Fig. 5, the model indicated that the optimum combustion reaction should occur when methanol was mixed with water at around 70% alcohol mixture (by volume). The results for the chemical species supported the trend above that the amount of oxygen gas was the lowest in the combustion area of 70% alcohol mixture. The products of the combustion process (water, carbon monoxide, and carbon dioxide) were found to be richest in the 70% alcohol mixture, not at 80% or above. This led to the conclusion that at this mixture, the combustion process occurred at the greatest efficiency since it consumed the maximum amount of reactant and released the maximum amount of products. The results from this model agreed well with the experimental results that a porous film was obtained from a 70% ethanol precursor solution while a powdery film was typically obtained from a higher percentage of ethanol in the precursor solution. The temperature contours also support this argument that their shapes are similar to the combustion zone *shape b* as proposed in Part 1.

When all the mixtures have vapourised and combusted, the first intermediate product of carbon was carbon dioxide. This carbon dioxide gas flew towards the substrate while in equilibrium with carbon monoxide gas when the temperature has reached its maximum. Carbon monoxide gas was in equilibrium with carbon dioxide gas over a short distance before being converted fully to carbon dioxide gas, although some of it reached the substrate.

8. Effect of droplet size

Fig. 7 showed the temperature distribution contours as a result of different droplet sizes from uniform size at (a) 10 microns, (b) 50 microns, and (c) 100 microns, and ranges of sizes from (d) 10–50 microns, (e) 10–100 microns, and (f) 50–100 microns when the mixture fraction was fixed at 0.2.

When different sizes and ranges of droplet size have been modelled, the temperature distribution patterns changed as shown in Fig. 7. If we consider the uniform size droplets in Fig. 7(a)–(c), all the combustions were incomplete from the temperature contours for the distance of interest. The smallest droplet size started combusting at a shorter distance from the spray nozzle to the larger size droplets, and the maximum temperature for smaller droplet sizes was also greater than that for the larger sizes. Therefore, a faster ignition and higher temperature flame was expected for smaller droplets, so that the overall combustion completed in a shorter period of

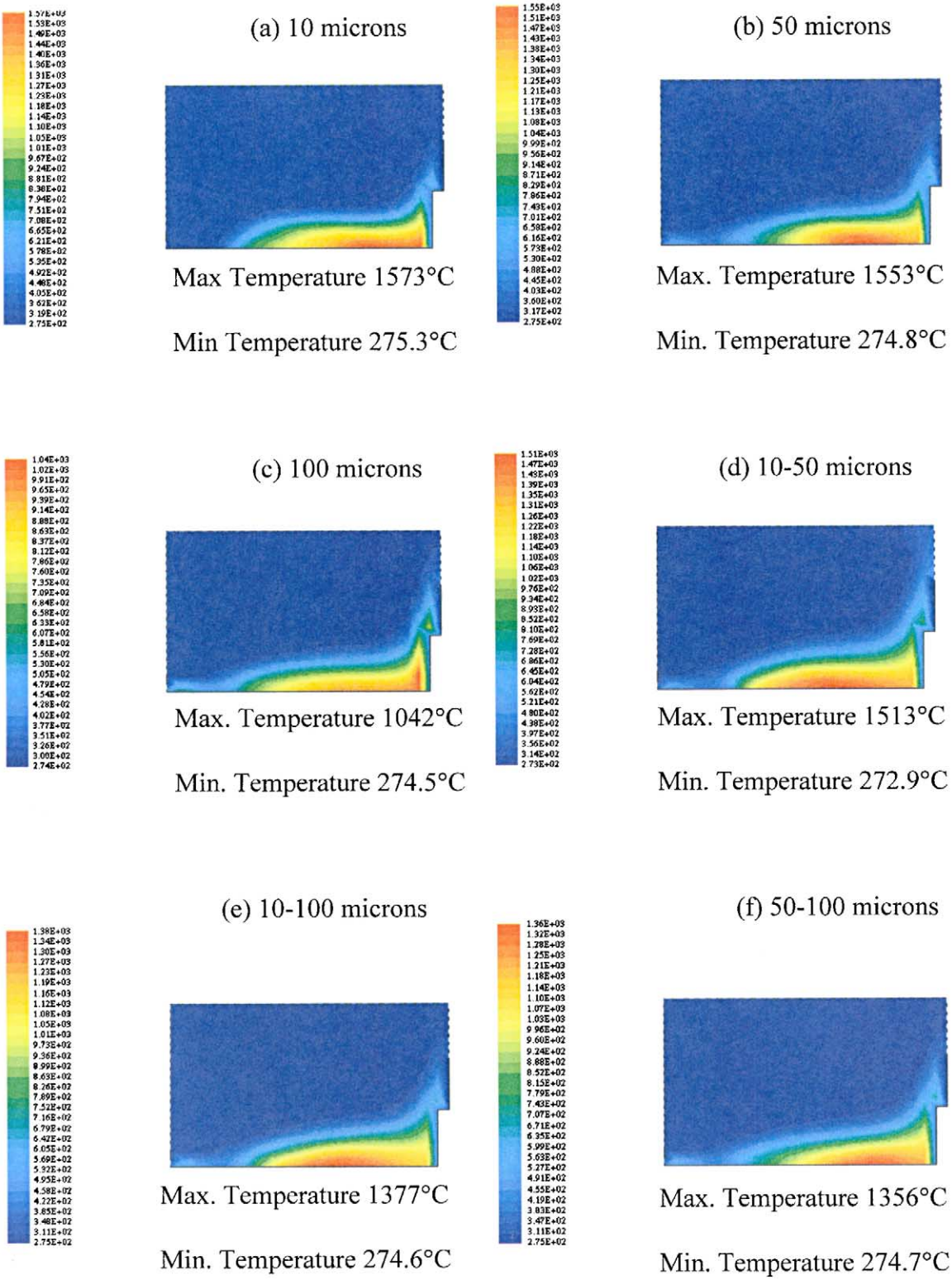

Fig. 7. Temperature distribution contours of various droplets size (a) 10, (b) 50, (c) 100, (d) 10–50, (e) 10–100, and (f) 50–100 microns when the mixture fraction was fixed at 0.2.

time. For the largest droplet size used here (100 microns), the combustion was not complete upon reaching the hot plate but continued on the walls, which was not desirable in real experiments.

When ranges of droplet size were considered, the shapes of the temperature contours were different from those of the uniform sizes that the contour shape was more tapered. The smaller size of droplet initiated the

combustion earlier and easier than the larger sizes. In Fig. 7(d) and (e) the combustion started at about the same distance while the combustion in Fig. 7(f) started at a distance further from the substrate. The maximum temperature of a droplet with size in the range 10–50 microns was slightly lower than those with uniform sizes of 10 microns and 50 microns. Particle size ranges of 10–100 and 50–100 microns gave maximum temperatures in between those of the uniformly small sizes (10 and 50 microns) and 100 microns.

A few small droplets caused early ignition, which increased the temperature and hence, increased the evaporation rate for the larger droplets. The whole ignition process then occured over a longer distance and a longer period of time.

The effect of droplet size could be compared with the effect of flow rate of the precursor solution (high flow rate produces large droplet size) and the air atomiser pressure (high pressure produces small droplet size) in Part 1. In the conditions of low flow rate of precursor solution (5.5 ml/min) and the high air atomiser pressure (26 psi), the deposited film was powdery because the combustion completed at a shorter distance than the condition for the larger droplet size.

It has been shown that a few large droplets or a few small droplets can have a significant effect on the results. The sensitivity of the process to the detailed spectrum of droplet sizes means that great care must be taken with this aspect of experimental setup.

9. Conclusions

The FAVD process was modelled using CFD techniques. The effect of changing three important process parameters was investigated. The results show good qualitative agreement with a parallel experimental study. The experimental and model parameters are correlated in the following way. The effect of mixture fraction, amount of fuel and the sizes of droplets are equivalent to the combination effect of the flow rate of fuel (precursor solution), ratio of alcohol to water, and air atomiser pressure in experiments. The complete combustion position in the model also indicates the suitable distance of the substrate from the spray nozzle of that particular combination of processing parameters.

Experimental results and theoretical considerations regarding the deposition process indicate that complete combustion at the substrate is desirable. Suitable process parameters indicated by the modelling work are given in Table 1 which are very close to the best combination of experimental parameters. It should be clear from this work that experiments and modelling can make complementary contributions to the understanding and optimisation of the FAVD process. It has been shown that FAVD can usefully be modelled using standard CFD techniques.

Table 1
Summary of optimum condition from modelling work

Mixture fraction	0.1–0.2
Amount of alcohol in the fuel	70%
Droplet size	10–50 microns

Acknowledgements

S. Charojrochkul wishes to express her gratitude to the Government of Thailand for the financial support through her PhD scholarship. Special thanks also go to Dr. C. Chanyavanich, Dr. J. Pearce, Dr. A. Manonukul and Associate Professor S. Assabumrungrat for useful discussion and comments

References

1. Choy, K. L. In *British Ceramic Proceedings*, ed. W. E. Lee, 1995, The Institute of Materials, London, pp. 65.
2. Wiedmann, I., Choy, K. L. and Derby, B., Novel synthesis and processing of ceramics. In *British Ceramic Proceedings*, ed. F. R. Sale. The Institute of Materials, London, 1994, pp. 133.
3. Choy, K. L., Charojrochkul, S. and Steele, B. C. H., Fabrication of cathode for solid oxide fuel cells using flame assisted vapour deposition technique. *Solid State Ionics*, 1997, **96**, 49–54.
4. Charojrochkul, S., Choy, K. L. and Steele, B. C. H., Cathode/electrolyte systems for solid oxide fuel cells fabricated using flame assisted vapour deposition technique. *Solid State Ionics*, 1999, **121**, 107–113.
5. Charojrochkul, S., Choy, K.L. and Steele, B.C.H., Flame assisted vapour deposition of cathode for solid oxide fuel cells: Part 1 Microstructure control from processing parameters. This journal.
6. Rudniak, L., Numerical simulation of chemical vapour deposition process in electric field. *Computers and Chemical Engineering*, 1998, **22**, S755–S758.
7. Harsta, A., Thermodynamic modelling of CVD of high-Tc superconductors. *J. Thermal Analysis*, 1997, **48**(5), 1093–1104.
8. Dekker, J. P., Moene, R. and Schoonman, The influence of surface kinetics in modelling chemical vapour deposition processes in porous preforms. *J. Mat. Sci.*, 1996, **31**(11), 3021–3033.
9. ACCESS CVD, software package for the simulation of chemical vapour deposition reactors by CHAM Ltd., Wimbledon, London, UK.
10. Kohse-Höinghaus, K., Löwe, A. and Atakan, B., Investigations of the gas phase mechanism of diamond diposition in combustion CVD. *Thin Solid Films*, 2000, **368**, 185–192.
11. Fluent User's Guide, Version 4.3, Fluent Inc., Lebanon, NH, 1995, Section 19, p. 41.
12. Fluent User's Guide, Version 4.3, Fluent Inc., Lebanon, NH, 1995, Section 19, p. 49.
13. Fluent User's Guide, Version 4.3, Fluent Inc., Lebanon, NH, 1995, Section 19, p. 93.
14. Charojrochkul, S., Evaluation of oxide cathodes fabricated via flame assisted vapour deposition technique, PhD thesis, Imperial College of Science, Technology and Medicine, University of London, London, 1998.
15. Hunt, A.T., Combustion chemical vapor deposition from liquid organic solutions. PhD thesis, Georgia Institute of Technology, GA, 1993.